

Cosmological Constant Effect on Charged and Rotating Black Hole Shadows

A. Belhaj^{1*}, M. Benali^{1†}, A. El Balali^{1‡}, W. El Hadri^{1§}, H. El Moumni^{2¶}

¹ Département de Physique, Equipe des Sciences de la matière et du rayonnement, ESMaR
Faculté des Sciences, Université Mohammed V de Rabat, Rabat, Morocco

² EPTHE, Physics Department, Faculty of Science, Ibn Zohr University, Agadir, Morocco

September 30, 2024

Abstract

Motivated by recent astrophysical observations, we investigate the shadow behaviors of four dimensional charged rotating black holes with a cosmological constant. This study is made in terms of a reduced moduli space parameterized by the charge and the rotation parameters. For fixed observers, we analyse in some details the shadow behaviors and the corresponding naked singularities of Kerr-Newman and Kerr-Sen four-dimensional black holes in Anti de Sitter backgrounds. Then, a comparative discussion is provided by computing the geometrical observables and the energy emission rate.

Keywords: Charged and rotating black holes, Cosmological constant, Shadows, Geometrical observables.

Mathematics Subject Classification: 83C57, 83B99, 83D99.

Contents

1	Introduction	2
2	Shadow behaviors of charged and rotating black holes	3
2.1	Shadows of Kerr-Newman AdS black hole	4

*a-belhaj@um5r.ac.ma

†mohamed_benali4@um5.ac.ma

‡anabelbalali@gmail.com

§elhadriwijdane4@gmail.com

¶h.elmoumni@uiz.ac.ma

¶ Authors in alphabetical order.

2.2	Shadows of Kerr-Sen AdS black hole	8
2.3	Naked singularity shadow	10
3	Distortion and energy emission rate: comparative study	12
3.1	Distortion behaviors	12
3.2	Energy emission rate	15
4	Effects of the cosmological constant on shadows	16
5	Conclusions and discussions	17

1 Introduction

Four dimensional black holes have received an increasing interest supported not only by many physical models including superstrings and related theories [1, 2], but also by the international Event Horizon Telescope (EHT) collaboration having unveiled the first shadow image of a supermassive black hole, located in the center of galaxy M87 [3, 4].

The strong evidence of the existence of supermassive black holes at the center of most galaxies in the universe, including the Milky Way [5], has supported several investigations in different models of gravity [6–9]. This includes braneworld black hole [10], Kerr-Newmann-NUT one [11], models with the cosmological constant where the usual formulae of geodesics, shadows, time of time delay and deflection angle. [12–15]. Considering the fact that universe is filled or dominated by a cosmological constant, the usual expression for gravitational lensing in Friedmann-Robertson-Walker geometries should be modified. In particular, the associated expressions need to be reanalyzed in order to check the cosmological observations [16–18]. On the other hand, a particular emphasis has been put on the interplay between such a physics on Anti-de-Sitter (AdS) geometries with a negative cosmological and thermodynamics. This has opened interesting windows to develop and elaborate many links with critical behaviors appearing in the black hole physics. Concretely, phase transitions of various AdS black holes have been extensively investigated showing non-trivial results. In this context, many thermodynamical quantities have been computed in order to unveil the thermodynamical properties of black holes obtained from different gravity theories [19, 20]. Four and higher dimensional concrete solutions have been dealt with by interpreting the cosmological constant as the pressure and its conjugate as the volume [21, 22]. Thermodynamics of charged and rotating AdS black hole systems, controlled generally by the mass, the charge and the angular momentum, have been approached using the physics of Van der Waals fluids. Superstring models and M-theory have been also exploited to investigate such properties by implementing other stringy fields including tensor and scalar fields [23–25]. More recently, optical properties of four-dimensional black holes have been largely stud-

ied in connections with non-trivial backgrounds completing the thermodynamical investigations [26–33]. Precisely, the shadows have been considered as a physical reality supported by EHT collaborations. For such reasons, shadow and deflection angle behaviors of various charged and rotating black holes have been discussed using different methods. In particular, it has been revealed that the shadows of non-rotating black holes involve a circular geometry. However, such a geometry can be deformed by introducing rotation parameters needed for engineering spinning solutions. In this models, the size of such a geometry depends also on certain parameters associated with external sources including dark energy (DE) and dark matter (DM) [34, 35]. A close inspection shows that the charged rotating AdS black hole shadows, in light of observations, could provide insight to the spacetime structure and information on the corresponding physics. In particular, the geodesics can be linked to two-point correlations in AdS/CFT context [36]. Therefore, the analysis of such shadows could be considered as a useful tool to not only explore the astrophysical black holes but also to compare alternative theories with general relativity. In [13–15], it has been focussed on angular radius of spherical black hole shadows with respect to comoving observers.

The aim of this work is to investigate the shadow behaviors of four-dimensional charged rotating black holes with a cosmological constant in terms of a reduced moduli space parameterized by the charge and the rotation parameters. Inspired by the recent work on the AdS backgrounds [37], we first elaborate, in some details, explicit models treating the Kerr-Newman (KN) solution and the Kerr-Sen (KS) black hole and the associated naked singularity shadow. Then, we discuss and compare the geometrical observables and the energy emission rate of both black holes. In this work, we use dimensionless units ($G = \hbar = c = 1$) and the recent method dealing with celestial coordinates for a cosmological constant backgrounds [11, 38, 39].

The paper is structured as follows. In section 2, we investigate the shadow behaviors of KN-AdS and KS-AdS black holes with a negative cosmological constant, respectively. Then, we discuss the naked singularity and its related shadow picture. In section 3, we analyse geometrical observable and the corresponding energy emission rate. In section 4, we inspect the cosmological constant effect on optical aspects for (A)dS backgrounds. The last section is devoted to conclusions and open questions

2 Shadow behaviors of charged and rotating black holes

In this section, we study the optical aspects of charged and rotating black holes in four dimensions. Concretely, we discuss the shadow geometrical pictures in terms of many parameters including the cosmological constant.

2.1 Shadows of Kerr-Newman AdS black hole

We start by considering the photon geodesics around the four-dimensional KN black hole with a cosmological constant, being a charged generalization of the Kerr black model. To get such a solution, one should exploit the Einstein-Maxwell modified action which reads as

$$\mathcal{I} = -\frac{1}{16\pi G} \int_M dx^4 \sqrt{-g} [R - F^2 - 2\Lambda], \quad (2.1)$$

where $F = dA$ denotes the field strength of the gauge potential 1-form. Λ is the cosmological constant. It is worth noting that two solutions can arise depending on Λ . For $\Lambda > 0$, the solution will be called Kerr-Newman de Sitter (KN-dS). However, $\Lambda < 0$ generates a solution referred to as Kerr-Newman Anti de Sitter (KN-AdS) which will be investigated in certain details through this work. As usually, the variation of the above action with respect to the metric tensor $g_{\mu\nu}$ can give KN solutions. According to [40, 41], the Boyer-Lindquist coordinates provide the following line element

$$ds^2 = -\frac{\Delta_r}{\Sigma} \left(dt - \frac{a}{\Xi} \sin^2 \theta d\phi \right)^2 + \Sigma \left(\frac{dr^2}{\Delta_r} + \frac{d\theta^2}{\Delta_\theta} \right) + \frac{\Delta_\theta \sin^2 \theta}{\Sigma} \left(a dt - \frac{(r^2 + a^2)}{\Xi} d\phi \right)^2,$$

where one has $\Sigma = r^2 + a^2 \cos^2 \theta$ and $\Xi = 1 + \frac{\Lambda}{3} a^2$. However, the Δ functions are given by

$$\Delta_\theta = 1 + \frac{\Lambda}{3} a^2 \cos^2 \theta, \quad \Delta_r = (r^2 + a^2) \left(1 - \frac{\Lambda r^2}{3} \right) - 2mr + Q^2. \quad (2.2)$$

Here, m , a and Q are the mass parameter, the angular momentum per unit mass and the charge, respectively. According to shadow black hole activities, the photon equation of motion on such a background can be elaborated using the Hamilton-Jacobi equation

$$\frac{\partial S}{\partial \tau} + \frac{1}{2} g^{\mu\nu} \frac{\partial S}{\partial x^\mu} \frac{\partial S}{\partial x^\nu} = 0, \quad (2.3)$$

where τ is the affine parameter associated with the geodesics. S being known by the Jacobi action is given by

$$S = -Et + L\phi + S_r(r) + S_\theta(\theta), \quad (2.4)$$

where $E = -p_t$ and $L = p_\phi$ are the conserved total energy and the conserved angular momentum of the photon, respectively, where p_μ is its four-momentum. They are geodesic constants of motion. $S_r(r)$ and $S_\theta(\theta)$ are functions depending only on r and θ variables, respectively. To get the complete relations of null geodesics, a separation method is needed which could be supported by the Carter mechanism [42, 43]. The illustration of the black hole shadow geometries requires two dimensionless impact parameters expressed as

$$\xi_{KN} = \frac{L}{E}, \quad \eta_{KN} = \frac{\mathcal{K}}{E^2}, \quad (2.5)$$

where \mathcal{K} denotes a separable constant analogue to the Carter one reported in [42]. The subscript KN stands for the Kerr-Newmann black hole solution. To obtain the corresponding

relations, certain calculations should be performed. Indeed, they give the null geodesics equations

$$\Sigma \frac{dt}{d\tau} = E \left[\frac{(r^2 + a^2) [(r^2 + a^2) - a\xi_{KN}\Xi]}{\Delta_r} + \frac{a (\xi_{KN}\Xi - a \sin^2 \theta)}{\Delta_\theta} \right], \quad (2.6)$$

$$\Sigma \frac{dr}{d\tau} = \sqrt{\mathcal{R}_{KN}(r)}, \quad (2.7)$$

$$\Sigma \frac{d\theta}{d\tau} = \sqrt{\Theta_{KN}(\theta)}, \quad (2.8)$$

$$\Sigma \frac{d\phi}{d\tau} = E \Xi \left[\frac{a((r^2 + a^2) - a\xi_{KN}\Xi)}{\Delta_r} + \frac{\xi_{KN}\Xi - a \sin^2 \theta}{\sin^2 \theta \Delta_\theta} \right]. \quad (2.9)$$

In these relations, $\mathcal{R}_{KN}(r)$ and $\Theta_{KN}(\theta)$ describing the radial and the polar motion read as

$$\mathcal{R}_{KN}(r) = E^2 \left[[(r^2 + a^2) - a\xi_{KN}\Xi]^2 - \Delta_r \eta_{KN} \right], \quad (2.10)$$

$$\Theta_{KN}(\theta) = E^2 \left[\eta_{KN} \Delta_\theta - \csc^2 \theta (a \sin^2 \theta - \xi_{KN}\Xi)^2 \right]. \quad (2.11)$$

It is known that the unstable circular orbit can determine the boundary of the black hole geometric shapes using the constraints

$$\mathcal{R}_{KN}(r) \Big|_{r=r_0} = \frac{d\mathcal{R}_{KN}(r)}{dr} \Big|_{r=r_0} = 0, \quad (2.12)$$

where r_0 represents the circular orbit radius of the photon [43–45]. By solving Eqs.(2.12) and taking into account $\Theta_{KN}(\theta) > 0$ for $0 \leq \theta \leq 2\pi$, we find

$$\eta_{KN} = \frac{16r^2 \Delta_r}{\Delta_r'^2} \Big|_{r=r_0}, \quad (2.13)$$

$$\xi_{KN} = \frac{(r^2 + a^2) \Delta_r' - 4r \Delta_r}{a \Xi \Delta_r'} \Big|_{r=r_0}, \quad (2.14)$$

where one has used the following derivation notation $\Delta_r' = \frac{\partial \Delta_r}{\partial r}$. In the presence of cosmological constant Λ , the position (r_{ob}, θ_{ob}) of the observer in Boyer-Lindquist coordinates should be fixed [39], where r_{ob} is the radial coordinate and θ_{ob} is angular coordinate. Assuming that the observer is in the domain of outer communication ($\Delta_r > 0$), and considering the trajectories of light rays sent from position (r_{ob}, θ_{ob}) to past, we explore the recent method reported in Ref [11, 38] to define the orthogonal tetrads (e_0, e_1, e_2, e_3) associated with the

observer position

$$e_0 = \frac{(r^2 + a^2)\partial_t + a\Xi\partial_\phi}{\sqrt{\Delta_r\Sigma}} \Big|_{(r_{ob}, \theta_{ob})}, \quad (2.15)$$

$$e_1 = \frac{\sqrt{\Delta_\theta}}{\sqrt{\Sigma}}\partial_\theta \Big|_{(r_{ob}, \theta_{ob})}, \quad (2.16)$$

$$e_2 = -\frac{a\sin^2\theta\partial_t + \Xi\partial_\phi}{\sqrt{\Delta_r\Sigma}\sin\theta} \Big|_{(r_{ob}, \theta_{ob})}, \quad (2.17)$$

$$e_3 = -\frac{\sqrt{\Delta_r}}{\sqrt{\Sigma}}\partial_r \Big|_{(r_{ob}, \theta_{ob})}. \quad (2.18)$$

In these relations, the timelike vector e_0 indicates the four-velocity of the observer. e_3 denotes the vector along the spatial direction pointing toward the center of the black hole. However, $e_0 \pm e_3$ are tangent to the direction of principal null congruences. The light ray can be expressed by the following parametrization

$$\lambda(s) = (r(s), \theta(s), \phi(s), t(s)). \quad (2.19)$$

In the way, the vector tangent to $\lambda(s)$, denoted by $\dot{\lambda}$, is given by

$$\dot{\lambda} = \dot{r}\partial_r + \dot{\theta}\partial_\theta + \dot{\phi}\partial_\phi + \dot{t}\partial_t. \quad (2.20)$$

Using the celestial coordinates ρ and δ as in [11], and the above basis vectors, $\dot{\lambda}$ can be written

$$\dot{\lambda} = \alpha(-e_0 + \sin\rho\cos\delta e_1 + \sin\rho\sin\delta e_2 + \cos\rho e_3), \quad (2.21)$$

where α is a scalar factor. Combining Eq.(2.20) and Eq.(2.21), one gets

$$\alpha = g(\dot{\lambda}, e_0) = \frac{1}{\sqrt{\Delta_r\Sigma}}(aL\Xi - (r^2 + a^2)E) \Big|_{(r_{ob}, \theta_{ob})}. \quad (2.22)$$

In order to find the celestial coordinates ρ and δ , we should exploit the equation Eq.(2.20) and Eq.(2.21). The coefficients of ∂_r and ∂_ϕ provide

$$\sin\rho = \sqrt{1 - \frac{\Sigma^2\dot{r}^2}{(E(r^2 + a^2) - aL\Xi)^2}} \Big|_{(r_{ob}, \theta_{ob})}, \quad (2.23)$$

$$\sin\delta = \frac{\sqrt{\Delta_\theta}\sin\theta}{\sqrt{\Delta_r}\sin\rho} \left(\frac{\Delta_r\Sigma\dot{\phi}}{E(r^2 + a^2) - aL\Xi} - a\Xi \right) \Big|_{(r_{ob}, \theta_{ob})}. \quad (2.24)$$

Using the above relations and implementing ξ_{KN} and η_{KN} via the equations of motion, one gets the celestial coordinates ρ and δ in terms of the parameters ξ_{KN} and η_{KN} as

$$\sin\rho = \frac{\pm\sqrt{\Delta_r\eta_{KN}}}{((r^2 + a^2) - a\xi_{KN}\Xi)} \Big|_{(r_{ob}, \theta_{ob})}, \quad (2.25)$$

$$\sin\delta = \frac{\sqrt{\Delta_r}\sin\theta}{\sqrt{\Delta_\theta}\sin\rho} \left(\frac{\Xi(a - \Xi\csc^2\theta\xi_{KN})}{a\Xi\xi_{KN} - (r^2 + a^2)} \right) \Big|_{(r_{ob}, \theta_{ob})}. \quad (2.26)$$

An examination shows that the boundary of shadows of such black holes depends on many parameters including cosmological constant numerical values. For simplicity reasons, we first consider the AdS backgrounds for which Λ is linked to the characteristic length scale of the AdS geometry via $\Lambda = -\frac{3}{\ell_{AdS}^2}$. For later use, we introduce a twist charge parameter $b = Q^2/2m$ in the associated Δ_r function. In this way, the shadow geometry will be controlled by a moduli space parameterized by $\{m, a, b\}$. Fixing the mass, such a space reduces to $\{a, b\}$. According to [11, 38, 39], the boundary of the shadow can be visualized using the cartesian coordinate system.

$$x = -2 \tan\left(\frac{\rho}{2}\right) \sin \delta, \quad (2.27)$$

$$y = -2 \tan\left(\frac{\rho}{2}\right) \cos \delta. \quad (2.28)$$

In Fig.(1), the associated shadow contours are plotted in such a plane by exploiting x and y expressions. In particular, we illustrate the shadow geometrical behaviors in terms of the (a, b) reduced moduli space. It has been observed that for very small values of the rotating parameter a the shadow shape involves a perfect circular geometry matching with non axisymmetric black hole shadow configurations. When such a rotation parameter becomes relevant, the black hole shadow is distorts by exhibiting a so-called D-shape form. It has been observed that the size depends on the b parameter. Indeed, it decreases by increasing b . Fixing the rotation parameter a , the shadow size is decreased by the increase of the parameter b .

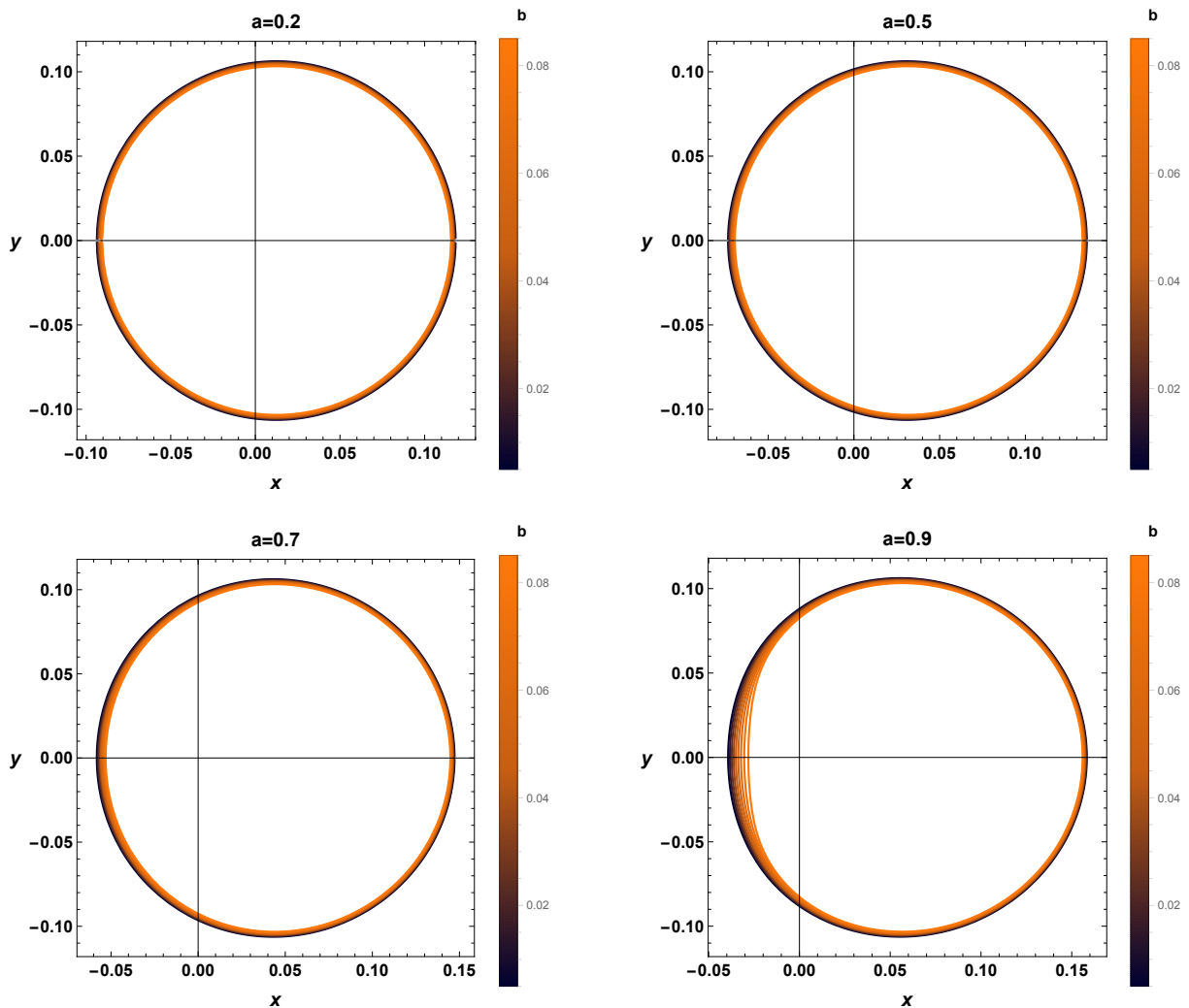


Figure 1: *Shadow behaviors of KN-AdS black holes for different values of a and b by taking $\Lambda = -10^{-4}$ and $m = 1$. The observer is positioned at $r_{ob} = 50$ and $\theta_{ob} = \frac{\pi}{2}$.*

2.2 Shadows of Kerr-Sen AdS black hole

Here, we deal with the shadow behaviors of the Kerr-Sen black hole with a negative cosmological constant built recently in [37]. We refer to this solution as KS-AdS. This solution has been obtained from the original KS model by implementing a nonzero negative cosmological constant [46]. It is known that this could be derived from a lower energy limit of the heterotic superstring theory living in ten dimension. Concretely, the associated black hole metric can be obtained from an action involving stringy fields, including the dilaton-axion field, a Maxwell field and the B-field. More details on the performed calculations can be found in [46]. Following [37], the line element the four dimensional KS-AdS black hole, in

the coordinates (t, r, θ, ϕ) , reads as

$$ds^2 = -\frac{\Delta_r}{\Sigma} \left(dt - \frac{a}{\Xi} \sin^2 \theta d\phi \right)^2 + \Sigma \left(\frac{dr^2}{\Delta_r} + \frac{d\theta^2}{\Delta_\theta} \right) + \frac{\Delta_\theta \sin^2 \theta}{\Sigma} \left(a dt - \frac{(r^2 + 2br + a^2)}{\Xi} d\phi \right)^2, \quad (2.29)$$

where the involved terms are given by

$$\Delta_r = \left(1 - \frac{(r^2 + 2br)\Lambda}{3} \right) (r^2 + 2br + a^2) - 2mr, \quad \Delta_\theta = 1 + \frac{a^2 \Lambda}{3} \cos^2 \theta, \quad (2.30)$$

$$\Xi = 1 + \frac{a^2 \Lambda}{3}, \quad \Sigma = r^2 + 2br + a^2 \cos^2 \theta. \quad (2.31)$$

It is indicated that m is a mass function and where a is a rotating parameter as before. While, the parameter b given $b = Q^2/2m$ denotes now the dilatonic scalar charge, playing the same role as the charge parameter of the KN black hole solution given in Eq.(2.2). Using similar techniques presented previously, the first-order differential equations, describing the photon motion in such a background, read as

$$\Sigma \frac{dt}{d\tau} = E \left[\frac{(r^2 + 2br + a^2) [(r^2 + 2br + a^2) - a\xi_{KS}\Xi]}{\Delta_r} + \frac{a (\xi_{KS}\Xi - a \sin^2 \theta)}{\Delta_\theta} \right], \quad (2.32)$$

$$\Sigma \frac{dr}{d\tau} = \sqrt{\mathcal{R}_{KS}(r)}, \quad (2.33)$$

$$\Sigma \frac{d\theta}{d\tau} = \sqrt{\Theta_{KS}(\theta)}, \quad (2.34)$$

$$\Sigma \frac{d\phi}{d\tau} = E \Xi \left[\frac{a((r^2 + 2br + a^2) - a\xi_{KS}\Xi)}{\Delta_r} + \frac{\xi_{KS}\Xi - a \sin^2 \theta}{\sin^2 \theta \Delta_\theta} \right]. \quad (2.35)$$

In these equations, $\mathcal{R}_{KS}(r)$ and $\Theta_{KS}(\theta)$ describing the radial and the polar motion take the following form

$$\mathcal{R}_{KS}(r) = E^2 \left[[(r^2 + 2br + a^2) - a\xi_{KS}\Xi]^2 - \Delta_r \eta_{KS} \right], \quad (2.36)$$

$$\Theta_{KS}(\theta) = E^2 \left[\eta_{KS} \Delta_\theta - \csc^2 \theta (a \sin^2 \theta - \xi_{KS}\Xi)^2 \right]. \quad (2.37)$$

Imposing the constraints $\mathcal{R}_{KS}(r)|_{r=r_0} = \frac{d\mathcal{R}_{KS}(r)}{dr}|_{r=r_0} = 0$ with $\Theta_{KS}(\theta) > 0$, the impact parameters ξ_{KS} and η_{KS} of the KS-AdS black hole can be obtained. Indeed, they are given by

$$\xi_{KS} = \frac{(r^2 + 2br + a^2)\Delta'_r - 4(r+b)\Delta_r}{a\Xi\Delta'_r} \Big|_{r=r_0}, \quad (2.38)$$

$$\eta_{KS} = \frac{16(b+r)^2\Delta_r}{\Delta_r'^2} \Big|_{r=r_0}. \quad (2.39)$$

Using similar computations, we obtain the scalar factor for such a black hole

$$\alpha = g(\dot{\lambda}, e_0) = \frac{1}{\sqrt{\Delta_r \Sigma}} (aL\Xi - (r^2 + 2br + a^2)E) \Big|_{(r_{ob}, \theta_{ob})}. \quad (2.40)$$

In this stringy solution, the celestial coordinates ρ and δ are given by

$$\sin \rho = \sqrt{1 - \frac{\Sigma^2 \dot{r}^2}{(E(r^2 + 2br + a^2) - aL\xi)^2}} \Big|_{(r_{ob}, \theta_{ob})}, \quad (2.41)$$

$$\sin \delta = \frac{\sqrt{\Delta_\theta} \sin \theta}{\sqrt{\Delta_r} \sin \rho} \left(\frac{\Delta_r \Sigma \dot{\phi}}{E(r^2 + 2br + a^2) - aL\xi} - a\xi \right) \Big|_{(r_{ob}, \theta_{ob})}. \quad (2.42)$$

Therefore, by the help of the above equations of motion, we can obtain the celestial coordinates ρ and δ in terms of the parameters ξ_{KS} and η_{KS} . Indeed, one finds

$$\sin \rho = \frac{\pm \sqrt{\Delta_r \eta_{KS}}}{((r^2 + 2br + a^2) - a\xi_{KS}\Xi)} \Big|_{(r_{ob}, \theta_{ob})}, \quad (2.43)$$

$$\sin \delta = \frac{\sqrt{\Delta_r} \sin \theta}{\sqrt{\Delta_\theta} \sin \rho} \left(\frac{\Xi(a - \Xi \csc^2 \theta \xi_{KS})}{a\xi_{KS} - (r^2 + 2br + a^2)} \right) \Big|_{(r_{ob}, \theta_{ob})}. \quad (2.44)$$

Taking the limit ℓ_{AdS} goes to the infinity, we recover the usual the KS black hole equations [47]. In order to visualise the shadows of KS-AdS black hole, we introduce the celestial coordinates ρ and δ in the equatorial plane as in the previous model. The corresponding behaviors in terms of the (a, b) reduced moduli space are plotted in Fig.(2). It follows from such a figure that the shadow shape is circular for slowly rotating black hole solutions. Moreover, its size depends on the b parameter. Indeed, it decreases by increasing b . It has been observed similar D-shapes as in the previous model for pertinent values of rotation parameter a .

Having discussed the shadow behaviors for real horizon radius values, we move to investigate other non-trivial configuration. It is known that when massive matter clouds undergo a continual gravitational collapse, the total mass collapses into a spacetime singularity. At such a location, the density, pressures and spacetime curvatures become infinite [48, 49]. In what follows, we consider the associated geometries.

2.3 Naked singularity shadow

Here, we would like to discuss the naked singularity shadow for both KN-AdS and KS-AdS black holes. Inspecting the shadow geometries, the unstable spherical orbits of the photons involves a circular geometry. In the naked singularity, however, such orbits are represented by arcs, as we will see. Due to the horizon absence, photons being close to both sides of the possible arcs can be seen by the observer [50, 51]. It is worth noting that the naked singularity appears when the largest root of $\Delta_r = 0$ takes complex values. In Fig.(3), we illustrate the

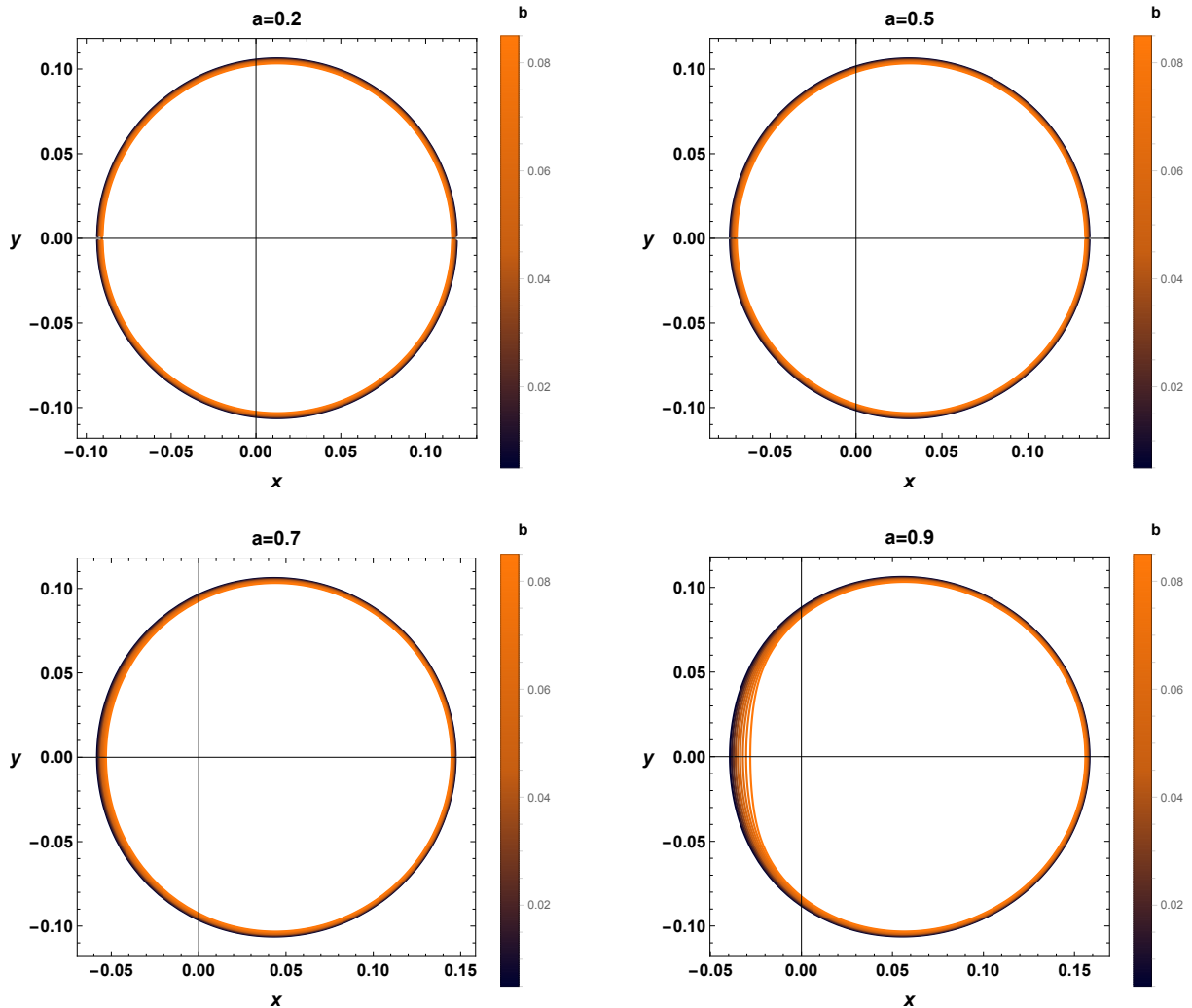


Figure 2: *Shadow behaviors of KS-AdS black holes for different values of a and b by taking $\Lambda = -10^{-4}$ and $m = 1$. The observer is positioned at $r_{ob} = 50$ and $\theta_{ob} = \frac{\pi}{2}$*

horizon region and the naked singularity for KN-AdS and KS-AdS black holes in terms of the parameters a and b . It has been observed that the horizon region of KS-AdS is bigger than KN-AdS. This result is also obtained for both black holes with vanishing cosmological constant [52]. The comparison of the results reported in [52] and the ones presented in Fig.(3) shows that the naked singularity region in Fig.(3) is larger.

An examination on such a solution shows that the b parameter is constrained by $0.125 \leq b \leq 0.405$. Considering such a bonded limit, the shadow as a function of the parameter b and a is plotted in Fig.(4). For small values of the rotating parameter, such a singularity appears only when $b > 0.325$ for both black holes. Taking $a = 0.9$, however, the naked singularity has been observed for the above parameter range.

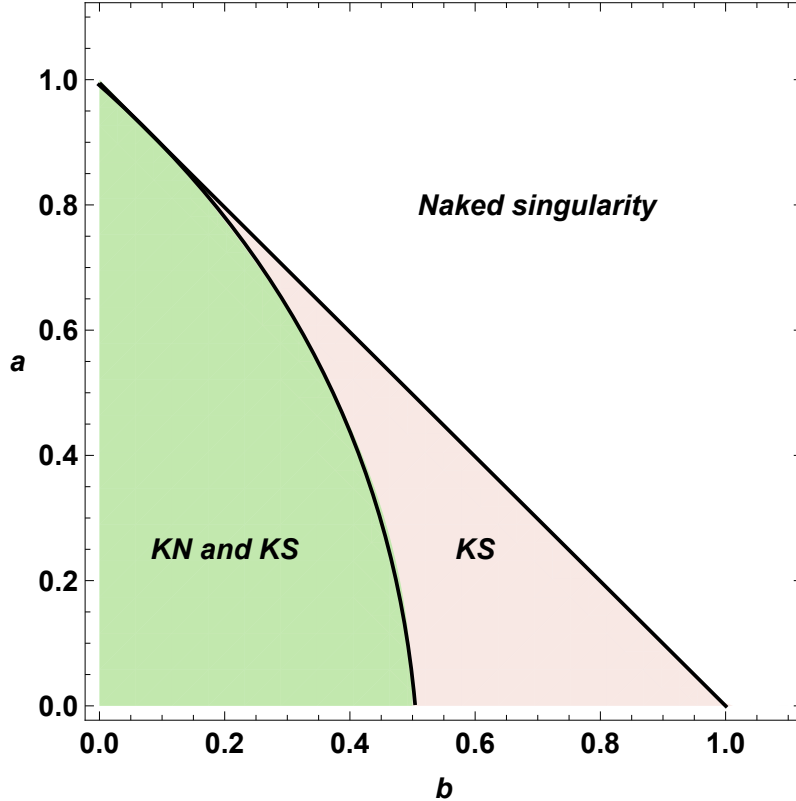


Figure 3: *Region plot for both KN-AdS and KS-AdS black holes as function of parameters a and b by taking $\Lambda = -10^{-4}$. The black solid lines correspond to extremal black hole cases.*

3 Distortion and energy emission rate: comparative study

In this section, we would like to provide a comparative study associated with a negative cosmological constant using certain regions of the (a, b) reduced moduli space. First, we start with the geometrical distortion behaviors. Then, we deal with the energetic aspects by examining the energy emission rate.

3.1 Distortion behaviors

To inspect the geometric deformations of the black hole shadows, one usually approach two parameters R_c and δ_c providing the size and the shape approximations, respectively [53, 54]. Precisely, the size is characterized by three specific points being top and bottom position of shadow (x_t, y_t) , (x_b, y_b) , the point of reference circle $(\tilde{x}_p, 0)$. In this way, the point of distorted shadow circle $(x_p, 0)$ meets the horizontal axis at x_p . Moreover, the distance between the two letter points is controlled by a parameter $D_c = \tilde{x}_p - x_p = 2R_c - (x_r - x_p)$ [54]. R_c is

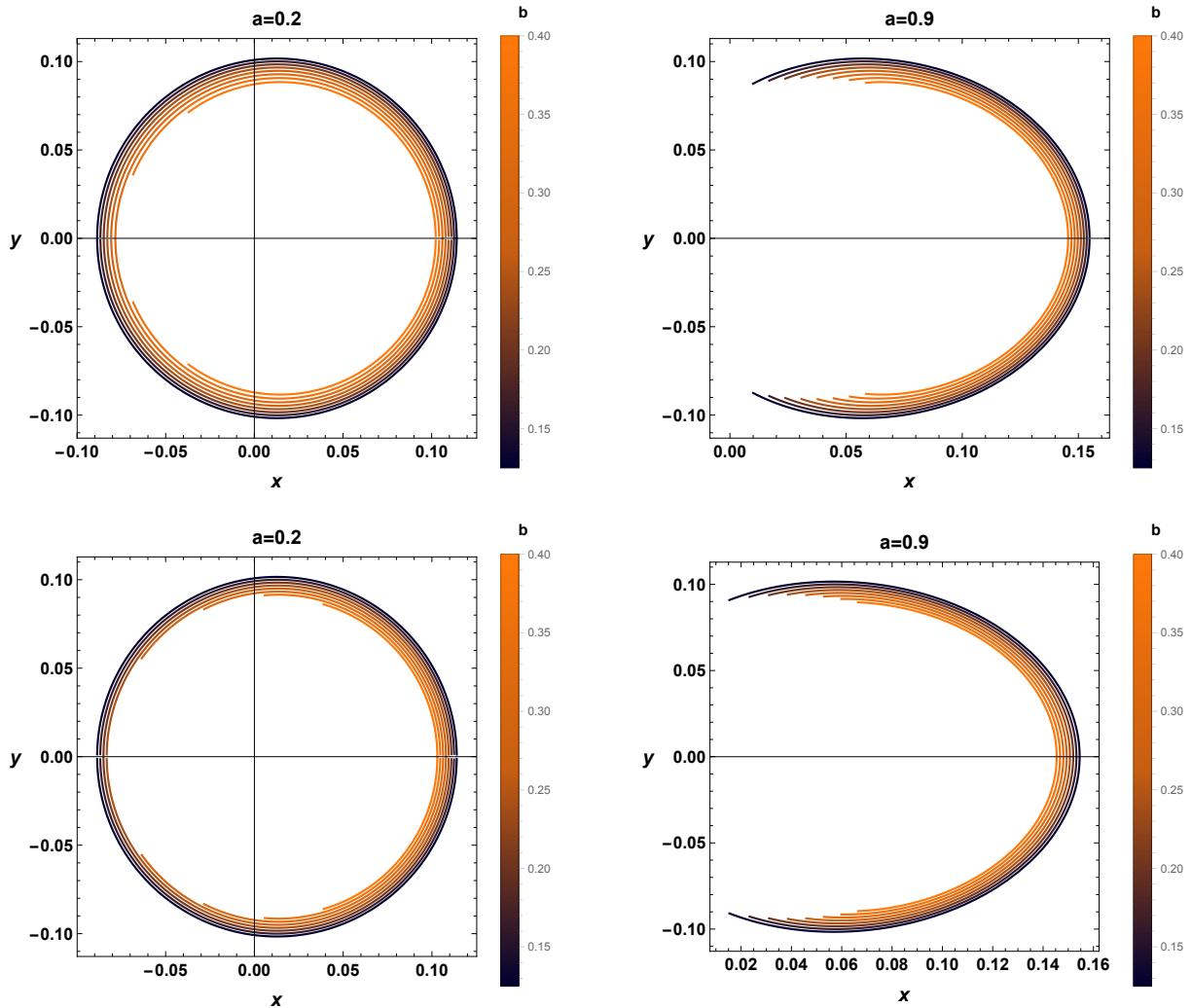


Figure 4: *Shadow behaviors of KN-AdS (top figure) and KS-AdS (bottom figure) black holes for different values of a and b by taking $\Lambda = -10^{-4}$ and $m = 1$. The observer is positioned at $r_{ob} = 50$ and $\theta_{ob} = \frac{\pi}{2}$.*

approximately given by

$$R_c = \frac{(x_t - x_r)^2 + y_t^2}{2|x_t - x_r|}. \quad (3.1)$$

However, the distortion parameter defined as a ratio of D_c and R_c is given by

$$\delta_c = \frac{|D_c|}{R_c}. \quad (3.2)$$

To provide a deep comparative study concerning the KN-AdS and the KS-AdS black holes, we analyse the astronomical parameters R_c and δ_c . These two observables are plotted in Fig.(5) in terms of the (a, b) reduced moduli space.

It has been observed that R_c , controlling the size, decreases by increasing the parameters b , R_c is almost the same for both black holes even if we vary the parameter a . For the value

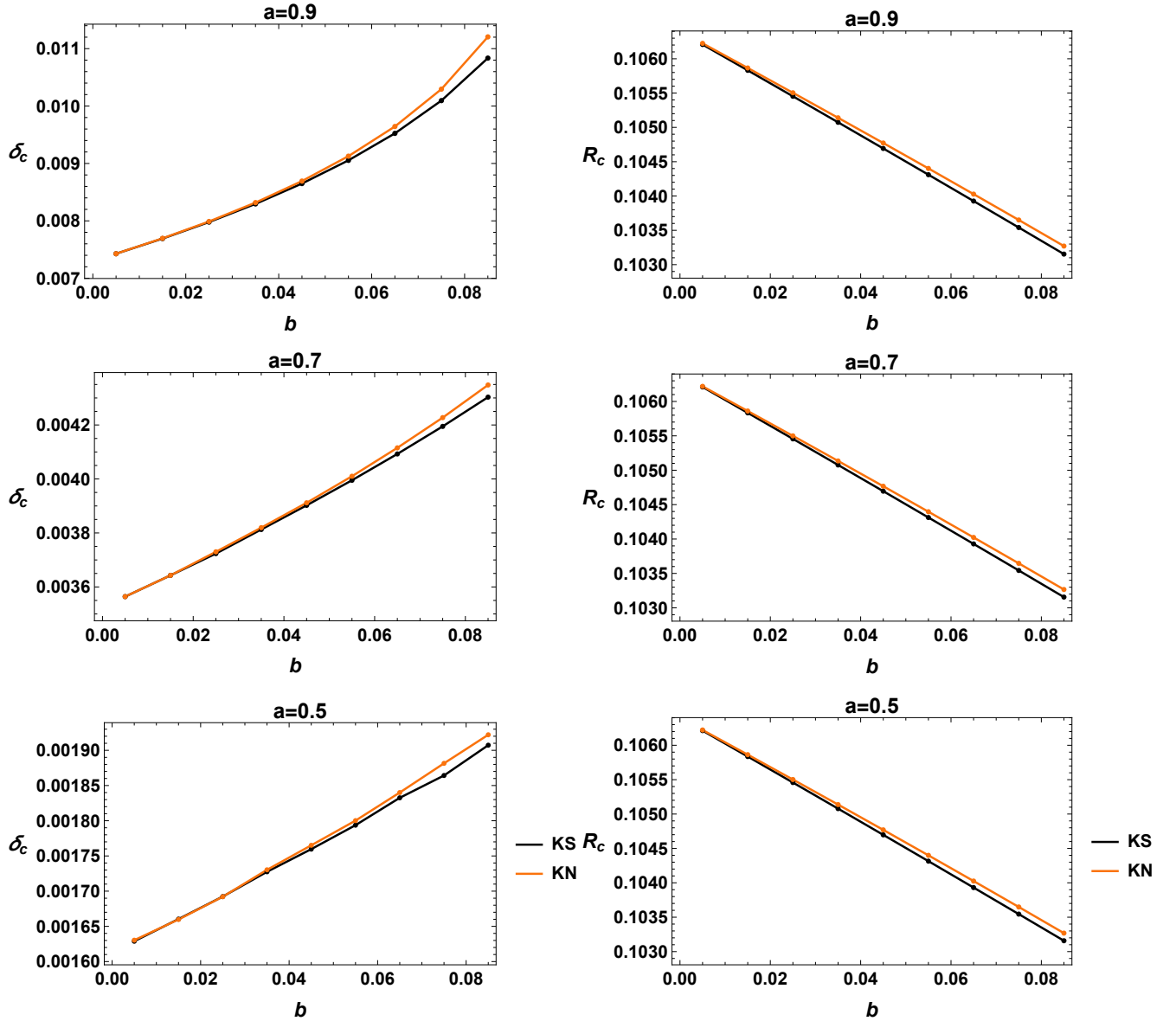


Figure 5: Astronomical observables for different values of b and a by taking $\Lambda = -10^{-4}$ and $m = 1$.

of b , between 0.005 to 0.09, R_c^{KS} and R_c^{KN} has almost same size for different values of a . Concerning the remaining astronomical parameter δ_c , controlling the distortion, it is plotted for both black holes in right panels of Fig.(5). It follows that for $a = 0.2$, the distortion parameter δ_c is almost zero for both types of black holes. For $a > 0.2$, δ_c increases by increasing the parameter a . It has been observed that δ_c^{KN} is bigger than δ_c^{KS} for values of b above 0.05. For values lower than 0.05, however, δ_c^{KN} and δ_c^{KS} are equal. For $b = 0.005$, the distortion δ_c of the two black holes coincides even if we vary the parameter a . Otherwise, δ_c^{KN} is bigger than δ_c^{KS} , showing that the distortion in the KN-AdS spacetime is more relevant than the one in the KS-AdS background.

Having discussed the shadow shapes of the rotating and charged black holes with a negative cosmological constant, we move to investigate the energy emission rate.

3.2 Energy emission rate

It has been known that for, a far distant observer, the absorption cross-section approaches to the black hole shadow. At very high energy, it is noted that the absorption cross-section oscillates near to a limiting constant value. According to [55], the later being approximately equal to the area of the black hole shadow ($\sigma \sim \pi R_c^2$) provides the energy emission rate expression given by

$$\frac{d^2 E(\varpi)}{d\varpi dt} = \frac{2\pi^3 (R_c^i)^2}{e^{\frac{\varpi}{T_i}} - 1} \varpi^3, \quad i = KN, KS \quad (3.3)$$

where ϖ is the emission frequency. In this relation, T_i which denote the temperature of the four-dimensional rotating and charged AdS black holes can be given in terms of the horizon radius r_h^i ($\Delta_r(r_h^i) = 0$). It has been observed that not all values of the temperature and the horizon radius are allowed for the the rotating AdS black hole due to the presence of the parameter a in the involved expressions. For the KS-AdS black hole, the temperature reads as

$$T_{KS} = \frac{1}{2\pi (a^2 + (r_h^{KS})^2)} \left(r_h^{KS} + b - \frac{(b + r_h^{KS}) (a^2 + 4br_h^{KS} + 2(r_h^{KS})^2) \Lambda}{3} - m \right). \quad (3.4)$$

In Fig.(6), we plot the energy emission rate as a function of the emission frequency ϖ for certain points of the (a, b) moduli space.

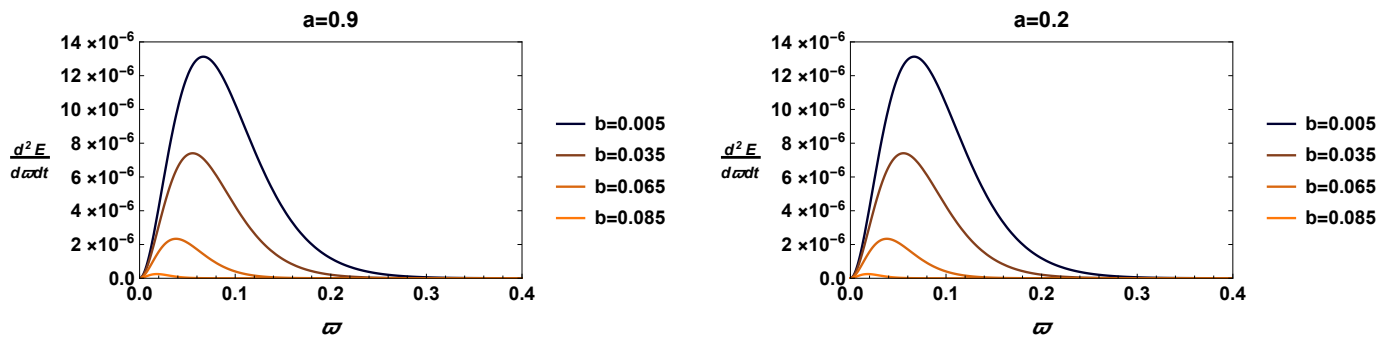


Figure 6: *Energy Emission rate for KS-AdS black hole for different values of b and a by taking $\Lambda = -10^{-4}$ and $m = 1$.*

It has been remarked from such a figure that the effect of the twist parameter b changes when we increase the rotation rate a . For $a = 0.2$, we concretely observe that the energy emission rate increases with the decrease in the value of the parameter b . For $a = 0.9$, however, the

same behavior is observed. Increasing the parameter a , the emission rate remains constant. For KN-AdS black hole, certain distinctions appear. Indeed, the Hawking temperature is given by

$$T_{KN} = \frac{1}{2\pi (a^2 + (r_h^{KN})^2)} \left(r_h^{KN} - \frac{r_h^{KN} (a^2 + 2(r_h^{KN})^2) \Lambda}{3} - m \right). \quad (3.5)$$

In Fig.(7), these energetic aspects are plotted as a function of the emission frequency ϖ for different values of a and b .

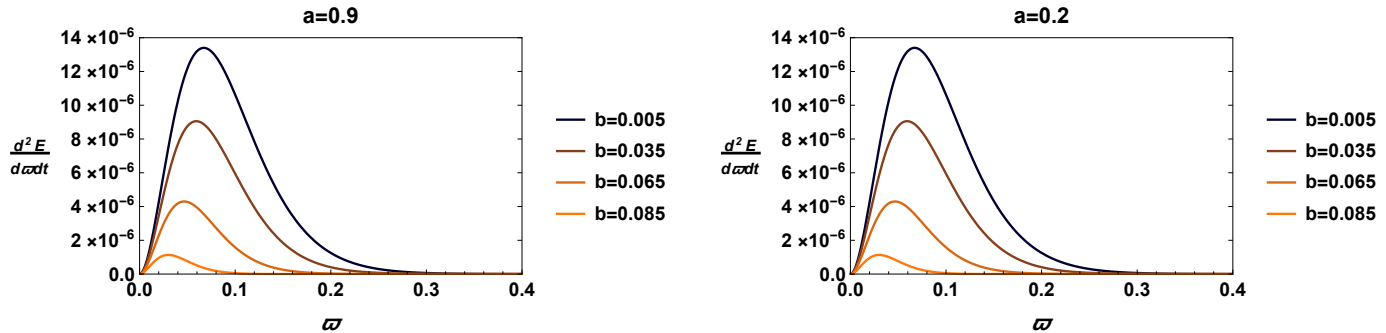


Figure 7: Energy emission rate of KN-AdS black hole for different values of b and a by taking $\Lambda = -10^{-4}$ and $m = 1$.

For small values of the rotation rate a , it has been seen from this figure that the KN-AdS black hole involves a slower evaporation process contrary to the KS-AdS one. Increasing the rotation rate parameter a , however, we remark that both black holes exhibit similar behaviors. This behavior of the energy emission can be clearly observed from the associated shadow radius and the temperature. This could be due to stringy effects on the black hole solutions. This suggestion could be addressed in future works.

4 Effects of the cosmological constant on shadows

In this section, we inspect the effects of the cosmological constant on shadows for both classes of charged rotating black holes. In Fig.(8), shadows with negative cosmological constant values for KN-AdS and KS-AdS are compared at particular points of the reduced moduli space.

It follows from this figure that the same shadow size for both black holes has been observed. Increasing the value of the cosmological constant, the shadow size decreases. It has been observed that the cosmological constant affects the shadow size. Moreover, a similar comparative discussion has been elaborated for zero cosmological constant at generic points of the moduli space associated with red circles. For small values, we recover the same result reported in [52].

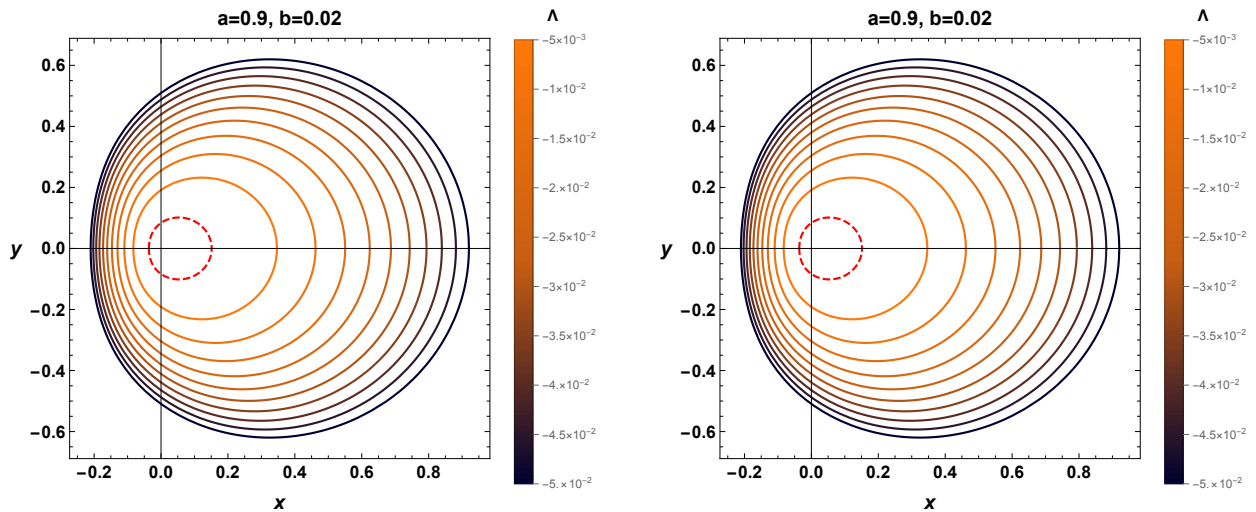


Figure 8: *Shadow behaviors of KN-AdS (left) and KN-AdS (right) for different values of the cosmological constant Λ for $m = 1$. In all panels, the red and dashed lines correspond to $\Lambda = 0$. The observer is positioned at $r_{ob} = 50$ and $\theta_{ob} = \frac{\pi}{2}$*

5 Conclusions and discussions

More recently, it has been remarked that the shadows of black holes has been considered as an active research subject encouraged by the finding of ETH international collaborations. Motivated by such activities, we have investigated the shadow of charged rotating black holes with a cosmological constant. For AdS geometries, we have elaborated two explicit models. First, we have studied shadow optical behaviors of the KN-AdS black holes. Then, we have discussed the naked singularity shadows for a constrained region of the moduli space. In order to unveil more data on such optical behaviors of charged rotating black holes with a negative cosmological constant, we have provided a comparative study. Precisely, we have found that the KN-AdS black hole possesses a small shadow radius compared to the KS-AdS one. These optical aspects have been consolidated by the energy emission rate and evaporation process. In such an investigation, relevant distinctions have appeared. Precisely, the KN-AdS energy emission rate is small compared to the KS-AdS one for some regions of the reduced moduli space (a, b) . Moreover, we have noticed that certain (a, b) regions have different effects on the KN-AdS black hole compared to the KS-AdS one.

A close examination reveals that the shadow of non-AdS KS and KN solutions have the same geometry. Moreover, this also includes the size for certain values of the rotation and the charge parameters [52]. This result has been recovered in the present study concerning the KS-AdS and KN-AdS solutions. For certain values of a and b , we have obtained the naked singularity geometry (an arc on the sky), which is the no domain of outer communication,

of two black hole solutions in the presence of a cosmological constant. A similar aspect has been observed for the Kerr–Newman–NUT black holes with a cosmological constant [11]. This paper comes up with many open questions. It would be of interest to inspect behaviors associated with non trivial backgrounds by considering either the effects of the spacetime dimension or external sources provided by DE and DM. It should be also interesting also to make contact with theoretical and observational findings. We hope to address elsewhere these open questions.

Acknowledgment

The authors would like to thank H. Belmahi, Y. Hassouni, K. Masmar, M. B. Sedra, A. Segui, and E. Torrente-Lujan for discussions on related topics. This work is partially supported by the ICTP through AF-13.

References

- [1] S. W. Hawking, *Black holes in general relativity*, *Communications in Mathematical Physics* 25(2) (1972) 152-166.
- [2] A. Strominger, C. Vafa, *Microscopic origin of the Bekenstein-Hawking entropy*, *Phys. Lett.* **B379** (2019) 99.
- [3] K. Akiyama *et al.* [Event Horizon Telescope], *First M87 Event Horizon Telescope Results. I. The Shadow of the Supermassive Black Hole*, *Astrophys. J.* **875**, no.1, L1 (2019), arXiv:1906.11238 [astro-ph.GA].
- [4] K. Akiyama *et al.* [Event Horizon Telescope], *First M87 Event Horizon Telescope Results. IV. Imaging the Central Supermassive Black Hole*, *Astrophys. J. Lett.* **875**, no.1, L4 (2019), arXiv:1906.11241 [astro-ph.GA].
- [5] . Gillessen and P. M. Plewa, F. Eisenhauer, R. Sari, I. Waisberg, M. Habibi, O. Pfuhl, E. George, J. Dexter, S. von Fellenberg, T. Ott, R. Genzel, *An Update on Monitoring Stellar Orbits in the Galactic Center*, *Astrophys. J.* **837**,30,(2017).
- [6] A. Awad and G. Nashed, *Generalized teleparallel cosmology and initial singularity crossing*, *JCAP* **02** (2017), 046 [arXiv:1701.06899 [gr-qc]].
- [7] W. El Hanafy and G. G. L. Nashed, *Exact Teleparallel Gravity of Binary Black Holes*, *Astrophys. Space Sci.* **361** (2016) no.2, 68 [arXiv:1507.07377 [gr-qc]].
- [8] G. G. L. Nashed, *Reissner Nordstrom solutions and Energy in teleparallel theory*, *Mod. Phys. Lett. A* **21** (2006), 2241-2250 [arXiv:gr-qc/0401041 [gr-qc]].

- [9] G. G. L. Nashed, *Stability of the vacuum nonsingular black hole*, Chaos Solitons Fractals **15** (2003), 841 [arXiv:gr-qc/0301008 [gr-qc]].
- [10] E. F. Eiroa and C. M. Sendra, *Shadow cast by rotating braneworld black holes with a cosmological constant* Eur. Phys. J. C **78**, no.2, 91 (2018) [arXiv:1711.08380 [gr-qc]].
- [11] A. Grenzebach, V. Perlick, C. Lämmerzahl, *Photon Regions and Shadows of Kerr-Newman-NUT Black Holes with a Cosmological Constant*, Phys. Rev. D **89**,(12) (2014) 124004.
- [12] B. Chandrasekhar and S. Mohapatra, *A Note on Circular Geodesics and Phase Transitions of Black Holes*, Phys. Lett. B **791**, 367-374 (2019) [arXiv:1805.05088 [hep-th]].
- [13] P. C. Li, M. Guo and B. Chen, *Shadow of a Spinning Black Hole in an Expanding Universe*, Phys. Rev. D **101** (2020) no.8, 084041 [arXiv:2001.04231 [gr-qc]].
- [14] Z. Chang and Q. H. Zhu, *Black hole shadow in the view of freely falling observers*, JCAP **06** (2020), 055 [arXiv:1911.02190 [gr-qc]].
- [15] O. Y. Tsupko, Z. Fan and G. S. Bisnovatyi-Kogan, *Black hole shadow as a standard ruler in cosmology*, Class. Quant. Grav. **37** (2020) no.6, 065016 [arXiv:1905.10509 [gr-qc]].
- [16] Z. Stuchlik and S. Hledik, *Some properties of the Schwarzschild-de Sitter and Schwarzschild - anti-de Sitter space-times*, Phys. Rev. D **60**, 044006 (1999)
- [17] G. V. Kraniotis and S. B. Whitehouse, *Exact calculation of the perihelion precession of mercury in general relativity, the cosmological constant and Jacobi's inversion problem*, Class. Quant. Grav. **20**, 4817-4835 (2003) [arXiv:astro-ph/0305181 [astro-ph]].
- [18] G. V. Kraniotis, *Precise relativistic orbits in Kerr space-time with a cosmological constant*, Class. Quant. Grav. **21**, 4743-4769 (2004) [arXiv:gr-qc/0405095 [gr-qc]].
- [19] N. Altamirano, D. Kubiznak, R. B. Mann, Z. Sherkatghanad, *Thermodynamics of rotating black holes and black rings: phase transitions and thermodynamic volume*, Galaxies **2** (2014) 89-159, arXiv:1401.2586 [hep-th].
- [20] A. Belhaj, M. Chabab, H. El Moumni, M. B. Sedra, *On Thermodynamics of AdS Black Holes in Arbitrary Dimensions*, Chin. Phys. Lett. **29** (2012)100401, arXiv:1210.4617 [hep-th].
- [21] B. P. Dolan, *Pressure and volume in the first law of black hole thermodynamics*, Class. Quant. Grav. **28** (2011) 235017, arXiv:1106.6260 [gr-qc].
- [22] D. Kubiznak, R. B. Mann, *P-V criticality of charged AdS black holes*, J. High Energy Phys. **1207** (2012) 033.

- [23] J. L. Zhang, R. G. Cai, H. Yu, *Phase transition and thermodynamical geometry for Schwarzschild AdS black hole in $AdS^5 \times S^5$ spacetime*, J. High Ener. Phys. **2** (2015) 143.
- [24] A. Belhaj, M. Chabab, H. El Moumni, K. Masmar, M. B. Sedra, *On thermodynamics of AdS black holes in M-theory*, Eur. Phys. J. **C76**(2) (2016) 73.
- [25] A. Belhaj, A. El Balali, W. El Hadri, Y. Hassouni, E. Torrente-Lujan, *Phase Transitions of Quintessential AdS Black Holes in M-theory/Superstring Inspired Models*, arXiv:2004.10647.
- [26] J. M. Bardeen, in Proceedings, Ecole d'Été de Physique Théorique: Les Astres Occlus: Les Houches, France, August, 1972 (1973) 215.
- [27] Z. Stuchlík and S. Hledík, *Some properties of the Schwarzschild–de Sitter and Schwarzschild–anti-de Sitter spacetimes*, Phys. Rev **D60**(1999) 044006.
- [28] J. L. Synge, *The Escape of Photons from Gravitationally Intense Stars* MNRAS, **131**(1966)463.
- [29] V. Perlick, O. Y. Tsupko, G. S. Bisnovatyi-Kogan, *Black hole shadow in an expanding universe with a cosmological constant*, Phys. Rev **D97**(2018)104062.
- [30] M. Zhang, M. Guo, *Can shadows reflect phase structures of black holes?*, arXiv:1909.07033 [gr-qc].
- [31] A. Belhaj, L. Chakhchi, H. El Moumni, J. Khalloufi, K. Masmar, *Thermal Image and Phase Transitions of Charged AdS Black Holes using Shadow Analysis*, arXiv:2005.05893 [gr-qc].
- [32] S. W. Wei, Y. C. Zou, Y. X. Liu, R. B. Mann, *Curvature radius and Kerr black hole shadow*, JCAP **08**, (2019)030, arXiv:1904.07710 [gr-qc].
- [33] H. Lu, H. D. Lyu, *Schwarzschild black holes have the largest size*, Phys. Rev. **D101**, no.4, (2020)044059, arXiv:1911.02019 [gr-qc].
- [34] A. Abdujabbarov, B. Toshmatov, Z. Stuchlík, B. Ahmedov, *Shadow of the rotating black hole with quintessential energy in the presence of plasma*, Int. J. Mod. Phys. **D26**, no.06, (2016) 1750051, arXiv:1512.05206.
- [35] S. Haroon, M. Jamil, K. Jusufi, K. Lin, R. B. Mann, *Shadow and Deflection Angle of Rotating Black Holes in Perfect Fluid Dark Matter with a Cosmological Constant*, Phys. Rev. **D99** (2019) 044015.
- [36] V. Balasubramanian, S. F. Ross, *Holographic particle detection*, Phys. Rev. **D 61**(2000) 044007, arXiv:hep-th/9906226 [hep-th].

- [37] D. Wu, P. Wu, H. Yu, S. Q. Wu, *Are ultra-spinning Kerr-Sen-AdS₄ black holes always super-entropic ?*, arXiv:2007.02224 [gr-qc].
- [38] S. Haroon, M. Jamil, K. Jusufi, K. Lin, R. B. Mann, *Shadow and Deflection Angle of Rotating Black Holes in Perfect Fluid Dark Matter with a Cosmological Constant*, Phys. Rev. D **99**,(12) (2019) 044015.
- [39] A. Grenzebach, V. Perlick, C. Lämmerzahl, *Photon Regions and Shadows of Accelerated Black Holes*, Int. J. Mod. Phys. D**24**,(09) (2015) 1542024.
- [40] B. Carter, *Hamilton-Jacobi and Schrodinger separable solutions of Einstein's equations*, Commun. Math. Phys. 10 (1968) 280.
- [41] J. F. Plebanski, M. Demianski, *Rotating, charged, and uniformly accelerating mass in general relativity*, Ann. Phys. **98** (1976) 98–127.
- [42] B. Carter, *Global structure of the kerr family of gravitational fields*. Physical Review, **174**(5) (1968)1559.
- [43] S. Chandrasekhar, *The mathematical theory of black holes*, volume 69. Oxford University Press, 1998.
- [44] A. Belhaj, M. Benali, A.E. Balali, H. El Moumni and S.-E. Ennadifi, *Deflection Angle and Shadow Behaviors of Quintessential Black Holes in arbitrary Dimensions*, Class. Quant. Grav. **37** (2020) 215004.
- [45] A. Belhaj, H. Belmahi, M. Benali, W. El Hadri, H. El Moumni and E. Torrente-Lujan, *Shadows of 5D Black Holes from string theory*, Phys. Lett. B **812** (2021) 136025.
- [46] A. Sen, *Rotating charged black hole solution in heterotic string theory*, Phys. Rev. Lett.**69**(7) (1992) 1006.
- [47] X. G. Lan, J. Pu, *Observing the contour profile of a Kerr–Sen black hole*, Mod. Phys. Lett. A **33**, no.17, (2018) 1850099.
- [48] P. M. Chesler, R. Narayan and E. Curiel, *Singularities in Reissner–Nordström black holes*, Class. Quant. Grav. **37** (2)(2020) , 025009, arXiv:1902.08323.
- [49] P. R. Brady, *The Internal Structure of Black Holes*, PTPS **136** (1999) 29.
- [50] A. de Vries, *The apparent shape of a rotating charged black hole, closed photon orbits and the bifurcation set A₄*, Class. Quant. Grav. 17, (2000)123.
- [51] L. Amarilla, E. F. Eiroa, *Shadow of a rotating braneworld black hole*, Phys. Rev. D **85** (2012) 064019.

- [52] S. V. M. C. B. Xavier, Pedro V. P. Cunha, Luís C. B. Crispino, Carlos A. R. Herdeiro, *Shadows of charged rotating black holes: Kerr-Newman versus Kerr-Sen*, Int. J Modern Phys. D **29** (2020)2041005.
- [53] K. Hioki, K. I. Maeda, *Measurement of the kerr spin parameter by observation of a compact object's shadow*, Phys. Rev. D, **80**(2)(2009)024042 .
- [54] M. Amir, S. G Ghosh, *Shapes of rotating nonsingular black hole shadows*, Phys. Rev. D**94**(2) (2016) 024054.
- [55] S. W. Wei, Y. X. Liu, *Observing the shadow of Einstein-Maxwell-Dilaton-Axion black hole*, JCAP **11** (2013)063, arXiv:1311.4251 [gr-qc].